Spin reorientation transition in layered perovskite $CaNdFeO_4$

2004 J. Phys.: Condens. Matter 16 8429

(http://iopscience.iop.org/0953-8984/16/46/028)

INSTITUTE OF PHYSICS PUBLISHING JOURNAL OF PHYSICS: CONDENSED MATTER

J. Phys.: Condens. Matter **16** (2004) 8429–8446 PII: S0953-8984(04)79752-0

Spin reorientation transition in layered perovskite $CaNdFeO_4$

Shigeaki Oyama[1], **Makoto Wakeshima**[1], **Yukio Hinatsu**[1] **and Kenji Ohoyama**[2]

[1] Division of Chemistry, Graduate School of Science, Hokkaido University, Sapporo 060-0810, Japan
[2] Institute for Materials Research, Tohoku University, Sendai 980-8577, Japan

Received 21 April 2004
Published 5 November 2004
Online at stacks.iop.org/JPhysCM/16/8429
doi:10.1088/0953-8984/16/46/028

Abstract

The spin-reorientation transition of layered perovskite oxide $CaNdFeO_4$ has been investigated through powder x-ray and neutron diffraction, magnetic susceptibility, specific heat and ^{57}Fe Mössbauer spectrum measurements. This oxide presents orthorhombic symmetry (space group: Bmab) with lattice parameters at room temperature $a = 5.4212(1)$ Å, $b = 5.4799(2)$ Å, and $c = 12.0617(2)$ Å. Through its magnetic susceptibility and specific-heat measurements, two magnetic anomalies were found at around 7 and 35 K. From ^{57}Fe Mössbauer spectra and neutron diffraction profiles of $CaNdFeO_4$, it has been elucidated that the anomalies observed at 7 and 35 K correspond to the antiferromagnetic ordering of the Nd^{3+} ion and a change in the direction of magnetic moment of the Fe^{3+} ion, respectively. The magnetic structures above and below the spin-reorientation transition temperature were determined. The spin-reorientation transition observed in $CaNdFeO_4$ has been induced by the onset of local magnetic interactions between the neodymium and iron sublattices.

1. Introduction

It is well known that some compounds with the K_2NiF_4-type structure [1–3] show interesting physical properties. These structures correspond to the case of $n = 1$ in the Ruddlesdon–Popper type structure for which the general formula is $AO(ABO_3)_n$, and are composed of alternating perovskite ABO_3 and rock salt AO layers along the c-axis. Hence, the important feature of the K_2NiF_4-type structures is the B–O–B bond of two-dimensional corner-sharing octahedral networks in the perovskite ABO_3 structure, and the compounds with this structure have two-dimensional magnetic properties.

A series of Ln_2MeO_4 (Ln = lanthanides, Me = transition metals) and $SrLnMeO_4$ are known to have K_2NiF_4-type structure. Most of their crystal structures have the ideal tetragonal

symmetry (space group: I4/mmm). However, it is also reported that the crystal structures of some K_2NiF_4-type compounds are distorted slightly from the ideal tetragonal symmetry, and that they change to have another tetragonal space group or orthorhombic symmetry [4–6].

We have been studying the magnetic properties of the layered perovskite-type oxide $SrNdFeO_4$ containing both strontium and neodymium [7]. It has been clear that the $SrNdFeO_4$ shows an antiferromagnetic transition of the Nd^{3+} moment at around 15 K and a change in the direction of magnetic moment of the Fe^{3+} moment at 36 K. Through powder neutron diffraction measurements, the magnetic structures below 300 K are determined, and it is elucidated that the direction of magnetic moment of the Fe^{3+} ion rotates by 90° from the *ab* plane to *c*-axis when the temperature is decreased by 36 K. Furthermore, the ordering of the Nd^{3+} moment also occurs below the same temperature. These results suggest that the spin-reorientation of the Fe^{3+} moments is induced by the local magnetic interactions between the Nd^{3+} and Fe^{3+} moments.

Here, we have paid attention to a compound $CaNdFeO_4$ in which Ca is substituted for Sr in the $SrNdFeO_4$. Previous structural investigations suggested that its crystal structure may not have tetragonal symmetry but orthorhombic symmetry [8]. In addition, the result of ^{57}Fe Mössbauer spectrum measurements on $CaLaFeO_4$ containing diamagnetic lanthanum showed an antiferromagnetic transition of the Fe^{3+} ion at 361 K [9]. However, detailed crystal structure and magnetic properties of $CaNdFeO_4$ have not been reported yet.

In this study, we have performed powder neutron diffraction, magnetic susceptibility, specific heat, and ^{57}Fe Mössbauer spectra measurements on the $CaNdFeO_4$ in order to elucidate its crystal structure and magnetic properties. Some interesting magnetic anomalies have been found, and their results are discussed here.

2. Experimental set up

The polycrystalline sample $CaNdFeO_4$ was prepared by a standard solid-state reaction. As starting materials, calcium carbonate ($CaCO_3$), neodymium sesquioxide (Nd_2O_3), and diiron trioxide (Fe_2O_3) were used. Nd_2O_3 was dried in advance at 1173 K before use. These reagents were weighed in appropriate metal ratios and ground into a fine powder in an agate mortar. The mixtures were pressed into pellets and then calcined in air at 1273 K for 12 h. After being cooled to room temperature, the pellets were reground, repressed, and heated in air at 1673 K for 48 h with regrinding and repelletizing.

The powder x-ray diffraction measurements were carried out from 15 K to room temperature in the range of $10^\circ \leqslant 2\theta \leqslant 120^\circ$ using a 2θ step size of 0.02° with Cu Kα radiation on a RINT2000 diffractometer (Rigaku, Japan). The sample was cooled down using a variable temperature cryostat system CryoMini (Iwatani Industrial Gases Co.). The powder x-ray diffraction measurements from 300 to 500 K were carried out on a MultiFlex diffractometer (Rigaku, Japan). The structure refinement was carried out by Rietveld analysis for the powder x-ray diffraction data with the program RIETAN2000 [10].

The powder neutron diffraction measurements were carried out at 2.5, 5, 10, 15, 20, 25, 30, 35, 40, 50, 60, 80, 95 K, and at room temperature in the range of $3^\circ \leqslant 2\theta \leqslant 153^\circ$ at intervals of 0.1° with a wavelength of 1.8207 Å. Measurements were performed on the Kinken powder diffractometer for high efficiency and high resolution measurements (HERMES) at the Institute for Materials Research (IMR), Tohoku University [11], installed at the JRR-3M Reactor in the Japan Atomic Energy Research Institute (JAERI), Tokai. The magnetic structures were determined by the Rietveld technique, using the program FullProf [12].

Magnetic susceptibility measurements were made using a SQUID magnetometer (Quantum Design, MPMS model). Susceptibility–temperature curves for each sample were

measured under both the ZFC (zero field-cooled) and FC (field-cooled) conditions. The former was measured on heating the sample to 400 K after zero-field cooling to 1.8 K and then applying a field of 1000 G. The latter was measured on cooling from 400 to 1.8 K at 1000 G. Additionally, the residual magnetization measurements were made in the temperature range from 5 to 400 K. The sample was cooled to 5 K after applying a field of 5 T at 400 K, then measured on heating to 400 K under zero-field.

Specific heat measurements were made using a relaxation technique with a heat capacity measurement system (Quantum Design, PPMS model) in the temperature range from 1.8 to 400 K. The sintered sample in the form of a pellet was mounted on a sample holder with Apiezon N grease (1.8–300 K) and H grease (270−400 K) for better thermal contact.

The ^{57}Fe Mössbauer spectra were measured from 15 to 550 K with a conventional transmissional Mössbauer spectrometer VT-6000 (Laboratory Equipment Co.) in the constant acceleration mode. Absorbers were prepared from finely ground $CaNdFeO_4$ which was weighed to give the optimum signal to noise ratio. A source of up to 100 mCi of ^{57}Co in Rh was used and the spectrometers were calibrated using α-iron at room temperature.

3. Results and discussion

3.1. Crystal structures

The results of the x-ray diffraction measurements show that the prepared material was $CaNdFeO_4$. A small amount of Nd_2O_3 was also present in this sample. Since the ratio of Nd_2O_3 was below 0.24 wt%, its effect on the magnetic property is negligibly small. The x-ray diffraction pattern of $CaNdFeO_4$ measured at room temperature is shown in figure 1, and the crystal structure has been analysed by the Rietveld method. The result indicates that $CaNdFeO_4$ has an orthorhombic K_2NiF_4-type structure (space group: Bmab) in which Ca^{2+} and Nd^{3+} ions are randomly distributed at the same Wyckoff 8f positions. The structural parameters obtained from Rietveld refinements at room temperature are summarized in table 1 and the crystal structure of $CaNdFeO_4$ is illustrated in figure 2(a). As seen in figure 2(b), the FeO_6 octahedra are tilted at the same angle clockwise and counterclockwise alternately in the [0 1 0] direction. Due to this tilting, the structure is orthorhombically distorted from ideal tetragonal symmetry and it can be quantified by using the α_1 and α_2 angles (see figure 2(b)); α_1 is the angle between the equatorial plane of the octahedron and the basal plane *ab* of the unit cell, and α_2 is the angle between the long axis of the octahedron O(2)–Fe–O(2) and the *c*-axis of the unit cell. These angles are slightly different at room temperature, α_1 being smaller than α_2. A similar tendency was reported for the case of the isomorphic $NdCaCrO_4$ and La_2NiO_4 [13, 14]. However, the values of α_1 and α_2 for $NdCaCrO_4$ and La_2NiO_4 are both smaller than those of $CaNdFeO_4$, which indicates a larger orthorhombic distortion for $CaNdFeO_4$ compared with that for $NdCaCrO_4$ and La_2NiO_4. In the K_2NiF_4-type structure, the calcium and neodymium atoms are nine-fold coordinated by oxygen atoms and the iron atom is six-fold coordinated. The selected interatomic distances are summarized in table 2. They indicate that the FeO_6 octahedron is tetragonally distorted. It is clear that the neodymium coordination polyhedron NdO_9 is strongly distorted with six different Nd–O distances. This distortion is due to the tilt of the FeO_6 octahedron.

The lattice parameters *a* and *b* show a peculiar temperature dependence, while the parameter *c* is constant below 50 K and increases monotonically with temperature above 100 K. Figure 3 shows the variation of lattice parameters *a* and *b* as a function of temperature. The value of the parameter *a* shows a broad minimum around 330 K, while the value of *b* shows a broad maximum around 300 K. Furthermore, both parameters *a* and *b* are almost constant at

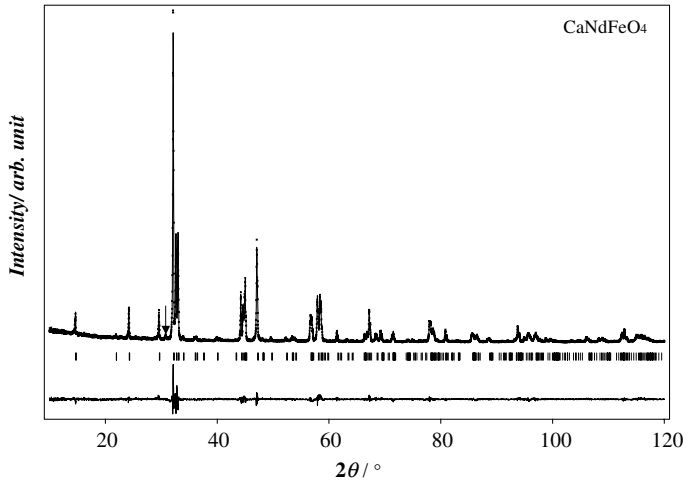

Figure 1. X-ray diffraction profiles for $CaNdFeO_4$. The calculated and observed diffraction profiles are shown by the top solid line and the cross markers, respectively. The vertical markers in the middle show positions calculated for Bragg reflections. The lower trace is a plot of the difference between calculated and observed intensities. An arrow in the profile corresponds to a diffraction peak for Nd_2O_3 impurity.

Table 1. Structural parameters of $CaNdFeO_4$ at room temperature obtained from Rietveld refinement of the x-ray diffraction data.

Space group: Bmab (No. 64)
$a = 5.4212(1)$ Å, $b = 5.4799(2)$ Å, $c = 12.0617(2)$ Å, $V = 358.33(1)$ Å^3
$\alpha_1 = 7.97(1)^\circ$, $\alpha_2 = 8.18(1)^\circ$
$R_{wp} = 12.21\%$, $R_I = 3.58\%$, $R_F = 2.65\%$

Atom	Site	Occupation	x	y	z	B (Å^2)
Ca,Nd	8f	1.0	0	−0.0120(3)	0.3576(1)	0.07(3)
Fe	4a	1.0	0	0	0	0.41(6)
O(1)	8e	1.0	1/4	1/4	−0.0160(7)	1.42(1)
O(2)	8f	1.0	0	0.0536(2)	0.1694(5)	1.42

Note: $R_{wp} = \left[\sum w(|F(\text{obs})| - |F(\text{cal})|)^2 / \sum w|F(\text{obs})|^2\right]^{1/2}$.
$R_I = \sum |I_k(\text{obs}) - I_k(\text{cal})| / \sum I_k(\text{obs})$.
$R_F = \sum |[I_k(\text{obs})]^{1/2} - [I_k(\text{cal})]^{1/2}| / \sum [I_k(\text{obs})]^{1/2}$.

low temperatures after a rapid decrease and increase of both the lattice parameters with decrease in temperature around 50 K. It seems reasonable to suppose that these anomalous temperature-dependences of the lattice parameters are due to the magnetostriction which is ascribable to the antiferromagnetic transition of the Fe^{3+} ions and the spin-reorientation transition of the Fe^{3+} magnetic moments. This has been ascertained by the ^{57}Fe Mössbauer spectrum and the powder neutron diffraction measurements, as will be described later.

3.2. Magnetic properties

Figure 4(a) shows the temperature dependence of the magnetic susceptibility below 60 K. In the inset of figure 4(a), the temperature dependence of the susceptibility is shown between

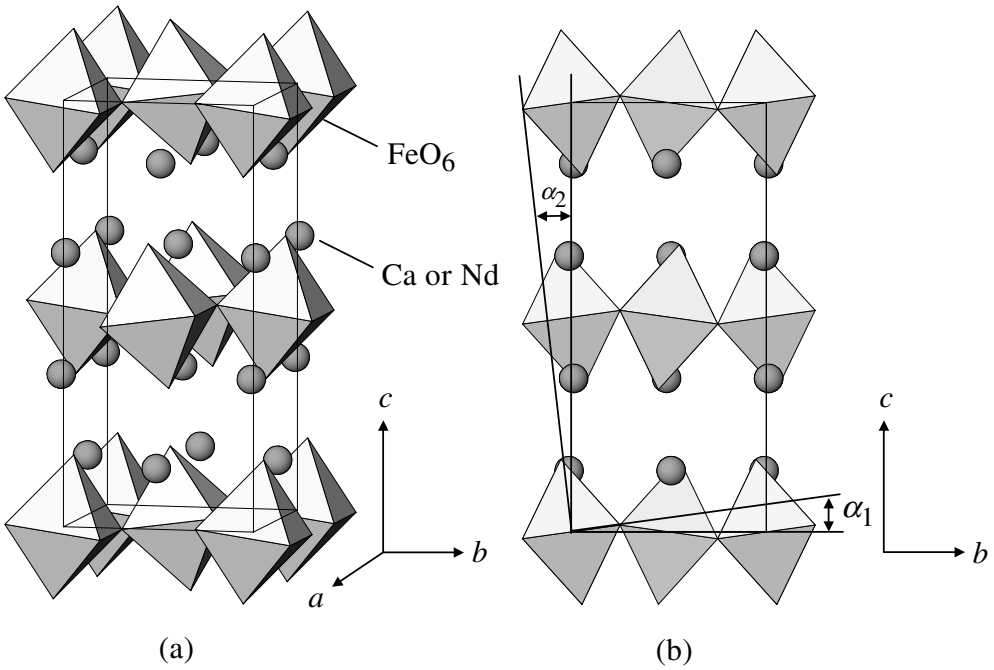

Figure 2. (a) The crystal structure of $CaNdFeO_4$. Spheres are Ca or Nd atoms, and octahedra are FeO_6 units. (b) View of the structure of $CaNdFeO_4$ from the a-axis, showing the tilt angles of FeO_6 octahedra.

Table 2. Selected interatomic distances (Å) at room temperature.

Ca,Nd–O(1)	×2	2.495(6)
Ca,Nd–O(1)	×2	2.681(6)
Ca,Nd–O(2)	×1	2.298(7)
Ca,Nd–O(2)	×1	2.403(9)
Ca,Nd–O(2)	×1	3.117(1)
Ca,Nd–O(2)	×2	2.740(1)
Fe–O(1)	×4	1.937(1)
Fe–O(2)	×2	2.065(7)
Fe–O(2)/Fe–O(1)		1.066

300 and 400 K. The susceptibility has a small anomaly around 370 K and the magnetic susceptibility does not follow a Curie–Weiss law below this temperature. From the Curie–Weiss fitting ($C/(T - \Theta_W) + \chi_{TIP}$, where χ_{TIP} is the temperature-independent term) to the χ–T curve above 380 K, the Curie constant (C) and the Weiss constant (Θ_W) are estimated to be 1.57(1) emu K mol^{-1} and $-25(3)$ K, respectively. The deviation from the Curie–Weiss law is due to the beginning of the long-range ordering of the layered Fe^{3+} sublattices with strong two-dimensional correlations, which is the characteristic magnetic behaviour found for many compounds with the K_2NiF_4-type structure. This two-dimensional correlation between the Fe^{3+} sublattices was already reported for the magnetic susceptibility of $CaLaFeO_4$ which depends only on the magnetic behaviour of the Fe^{3+} ions [15]. Magnetic susceptibility of $CaLaFeO_4$, is almost temperature-independent for temperatures for which the Fe^{3+} moment shows a long-range antiferromagnetic ordering [15]. On the assumption that

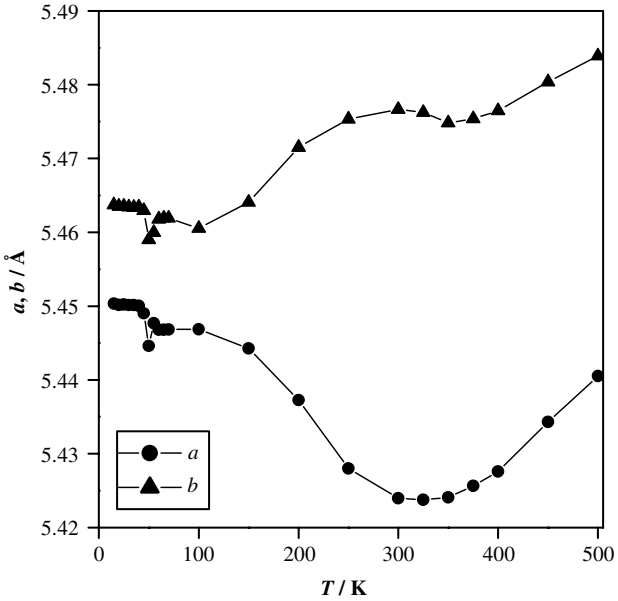

Figure 3. Temperature dependence of the lattice parameters a and b of $CaNdFeO_4$.

the magnetic susceptibility of the Fe^{3+} moments for $CaNdFeO_4$ is temperature-independent in the temperature range of 380–400 K, the obtained Curie constant corresponds to that of Nd^{3+} ions. The effective magnetic moment ($3.54\mu_B$) calculated from the Curie constant (1.57 emu K mol^{-1}) agrees well with the theoretical value ($3.62\mu_B$) of free Nd^{3+} ion.

In the plot of the magnetic susceptibility against temperature, three anomalies have been observed. The small anomaly around 370 K is due to the long-range antiferromagnetic ordering of the Fe^{3+} sublattice as will be revealed by the ^{57}Fe Mössbauer spectra (section 3.3). The ZFC magnetic susceptibility shows a broad maximum at 7 K and decreases with decreasing temperature, indicating the occurrence of a long-range antiferromagnetic ordering. Since the magnetic moments of the Fe^{3+} sublattice order at 360 K, the antiferromagnetic transition observed at 7 K should be due to the magnetic ordering of the Nd^{3+} moments. This contrasts with the results of the magnetic susceptibility measurements on the isomorphic K_2NiF_4-type oxide $NdCaCrO_4$ which shows short-range magnetic correlations of the antiferromagnetic characteristic within the Nd^{3+} sublattice [13]. On the other hand, our neutron diffraction measurements show that $CaNdFeO_4$ has a long-range magnetic interaction within the Nd^{3+} sublattice, which will be described later.

In the χ–T curve (figure 4(a)), another maximum has been found at 35 K and below this temperature the difference between the ZFC and FC susceptibilities was observed. Figure 4(b) shows the temperature dependence of the residual magnetization of the FC susceptibility for $CaNdFeO_4$. The residual magnetization suddenly increases when the temperature is decreased through 35 K, indicating the existence of a ferromagnetic component. However, it is difficult to explain the origin of its ferromagnetic component because of its too small residual magnetization ($\sim 1.0 \times 10^{-3}\mu_B$) at 5 K. It may be a weak ferromagnetic component arising from the canted-antiferromagnetic spin arrangement of the Fe^{3+} magnetic moments.

To resolve the anomalies of the magnetic susceptibility, specific heat measurements have been performed. Figure 5(a) shows the variation of the specific heat (C_p) for $CaNdFeO_4$ as a

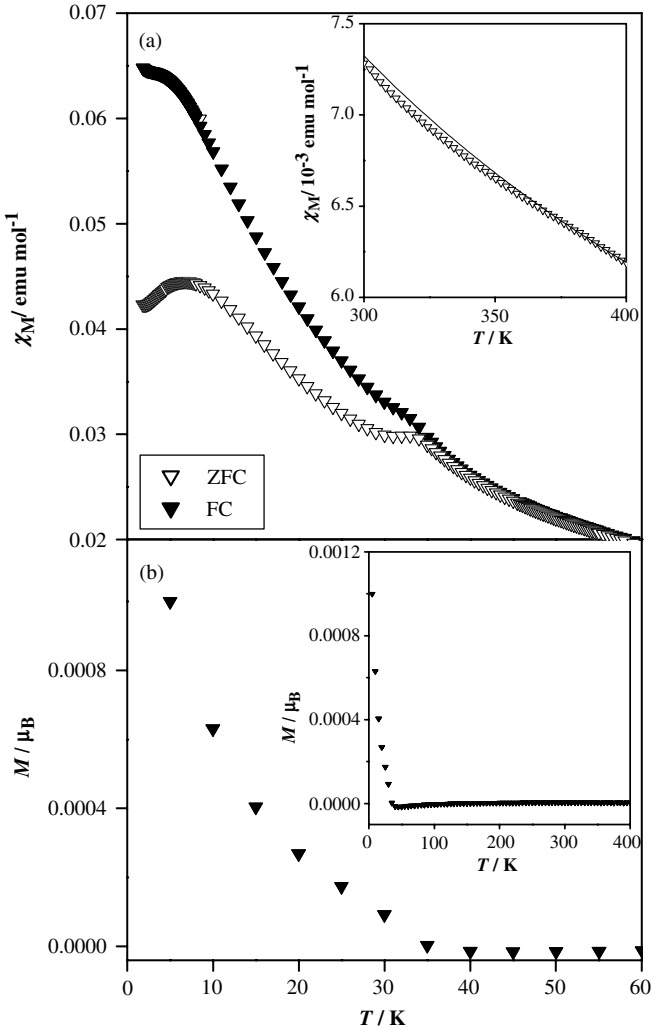

Figure 4. (a) Temperature dependence of the magnetic susceptibility of $CaNdFeO_4$ below 60 K. The magnetic susceptibility in the temperature range of 300–400 K is shown in the inset. ——, Curie–Weiss fitting in the temperature range from 380 to 400 K (see text). (b) Temperature dependence of the residual magnetization of $CaNdFeO_4$ below 60 K. The inset shows the residual magnetization in the temperature range of 1.8–400 K.

function of temperature. The specific heats show the existence of one very broad anomaly over the wide temperature range from 320 to 380 K, and two anomalies observed at 7 and 35 K. The very broad anomaly observed at 320–380 K is due to a long-range antiferromagnetic ordering of the Fe^{3+} ions. For layered perovskite-type compounds A_2BO_4, since a short-range ordering in the ABO_3 layer should develop well above the temperature at which three-dimensional magnetic ordering occurs, a broad anomaly or no anomaly is observed in the temperature dependence of the specific heat [16, 17]. The specific heats of $CaNdFeO_4$ also indicate that the magnetic coupling among the Fe^{3+} moments in the $(Ca,Nd)FeO_3$ layers is much stronger than that between the $(Ca,Nd)FeO_3$ layers.

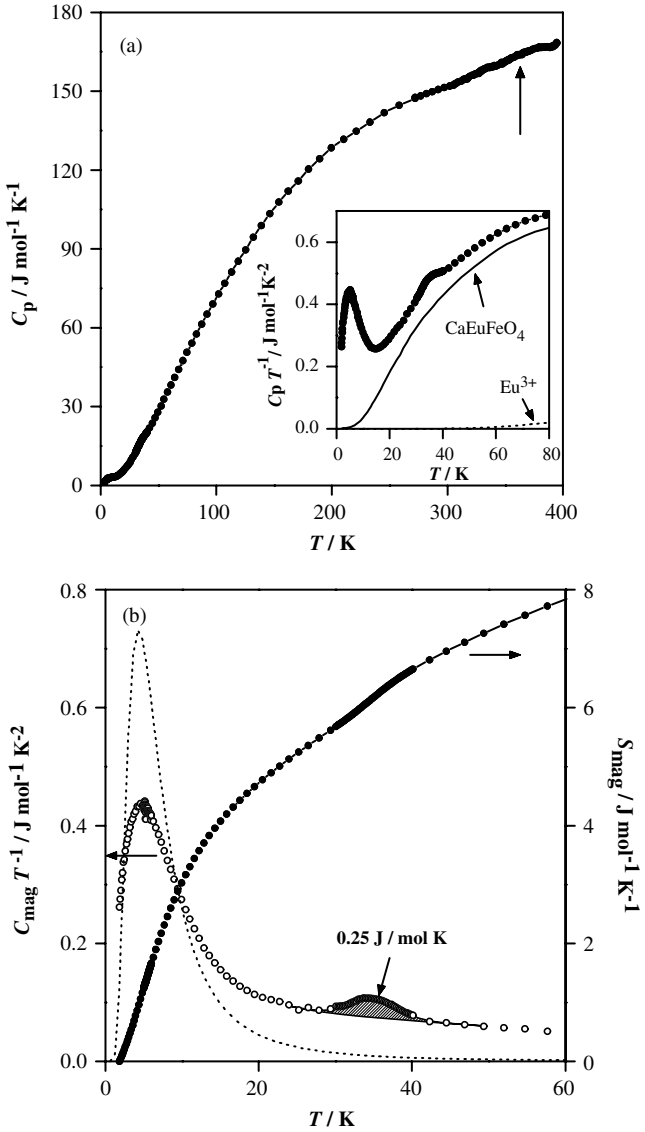

Figure 5. (a) Temperature dependence of the specific heat (C_p) of $CaNdFeO_4$. An arrow in the C_p–T curve corresponds to a broad anomaly due to an antiferromagnetic ordering of the Fe^{3+} ions. The C_pT^{-1}–T curve of $CaNdFeO_4$ is shown in the inset. ——, C_pT^{-1} of $CaEuFeO_4$; - - - -, calculated Schottky anomaly, which is attributable to the excited states ^7F_J ($J = 1, 2, \ldots, 6$) of Eu^{3+}, on the assumption that the energy splitting between the ground state ($^7F_0$) and the first excited state ($^7F_1$) is 500 K. (b) Temperature dependence of $C_{mag}(Nd^{3+})/T$ and $S_{mag}(Nd^{3+})$ for $CaNdFeO_4$. A dotted curve shows the calculated two-level Schottky curve $(C_{Sch}/T) - T$ with the energy splitting of 14 K. The area shaded with slanting lines represents the contribution of the spin-reorientation. The entropy change is estimated to be 0.25 J mol^{-1} K^{-1}.

In order to estimate the magnetic contribution (C_{mag}) of the Nd^{3+} moments to C_p at low temperatures, we need to subtract the lattice contribution (C_{lat}), the electronic contribution ($C_e \sim 0$ J mol^{-1} K^{-1} for insulators), and C_{mag} of the Fe^{3+} moments from the total C_p. The C_p/T data for insulating $CaEuFeO_4$, which is isostructural with $CaNdFeO_4$, are also plotted

in the inset of figure 5(a). For the Eu^{3+} ions, the energy difference between the ground state ($^7F_0$) and the first excited state ($^7F_1$) is roughly 500 K [18]. Therefore, we can assume that the population of the 'nonmagnetic' $^7F_0$ state is predominant at low temperatures and that the Schottky-type specific heat contributions, which are attributable to the excited states ^7F_J ($J = 1, 2, \ldots, 6$), to the total C_p of $CaEuFeO_4$ are negligible below 60 K (see the inset of figure 5(a)). In addition, for $CaEuFeO_4$, a long-range antiferromagnetic ordering of Fe^{3+} occurs at ~330 K [19]. Therefore, we can assume that the C_{lat} and $C_{mag}(Fe^{3+})$ contributions to the total C_p of $CaEuFeO_4$ are almost the same as those of $CaNdFeO_4$ below 60 K. The $C_{mag}(Nd^{3+})$ for $CaNdFeO_4$ is obtained by subtracting the total C_p of $CaEuFeO_4$ from that of $CaNdFeO_4$. The temperature dependences of C_{mag}/T and the magnetic entropy ($S_{mag} = \int_0^T (C_{mag}/T')\,dT'$) below 60 K are shown in figure 5(b).

In the C_{mag}/T versus T curve, two broad anomalies appear around 7 and 35 K. These anomalies correspond to the magnetic anomalies observed in the χ–T curve of figure 4(a). The magnetic anomaly at 35 K is due to the spin-reorientation of the Fe^{3+} magnetic moments [7], as will be described in sections 3.3 and 3.4. The entropy change for this spin-reorientation is estimated to be 0.25 J mol^{-1} K^{-1} (see figure 5(b)) and this value is consistent with those of other compounds, which support the spin-reorientation of the Fe^{3+} moments (0.3 J mol^{-1} K^{-1} for $TbFeO_3$ [20], 0.7 J mol^{-1} K^{-1}for $YbFeO_3$ [20], and 0.47 J mol^{-1} K^{-1} for $SrNdFeO_4$ [19]). The $^4I_{9/2}$ ground state of the Nd^{3+} ion should split into five Kramers doublets by crystal electric field effects in an orthorhombic symmetry. From features of the broad maximum at 7 K, one expects that this anomaly corresponds to a two-level Schottky-type specific heat for the low-lying doublet of the Nd^{3+} ion split by the molecular field of the ordered Fe^{3+} moments, as shown in $NdFeO_3$ [21], $NdCrO_3$ [22], and $NdCrO_4$ [23]. However, we could not fit the two-level Schottky-like curve to the measured (C_{mag}/T)–T curve. The dotted curve in figure 5(b) depicts the calculated two-level Schottky curve with a level splitting at 14 K. Compared with this calculated curve, the measured C_{mag}/T has a lower maximum and a larger tail at high temperatures. The Nd^{3+} moments are found to order magnetically below 35 K through neutron diffraction measurements (see section 3.4). The discrepancy between the measured and calculated C_{mag} might be due to the antiferromagnetic ordering of the Nd^{3+} moments. From the S_{mag}–T curve, the magnetic entropy change increases gradually with temperature, reaching 5.7 J mol^{-1} K^{-1} at 30 K. Because S_{mag} approaches $R \ln 2 \sim 5.8$ J mol^{-1} K^{-1}, where R is the gas constant, it is found that the low-lying doublet forms predominantly the antiferromagnetic state of the Nd^{3+} moments.

3.3. ^{57}Fe Mössbauer spectra

Figure 6 shows the ^{57}Fe Mössbauer spectra of $CaNdFeO_4$ at 15, 30, 40, 50, 360 and 370 K. A doublet in the spectrum at 370 K indicates that the Fe^{3+} ions occupy one site (the 4*a* site of space group Bmab) in $CaNdFeO_4$ and are in a paramagnetic state at this temperature. A decrease in the intensity of the doublet with decreasing temperature and an appearance of broad peaks in the spectrum at 360 K reveal the occurrence of a long-range magnetic ordering of the Fe^{3+} moment, and a sextet appeared in the spectra measured below this temperature shows an antiferromagnetic state of the Fe^{3+} moments. The doublet in the spectrum at 370 K is indicative of an electric quadrupole interaction between the electric field gradient and the electric quadrupole moment of the Fe^{3+} ions with a crystallographic point group C_{2h} in $CaNdFeO_4$.

Figure 7 shows the temperature dependence of the isomer shifts of the Fe^{3+} ion for $CaNdFeO_4$. The isomer shift δ at 300 K is determined to be 0.28(4) mm s^{-1}. This value is appropriate, because the isomer shifts for the high-spin state ($S = 5/2$) of the Fe^{3+} ion with

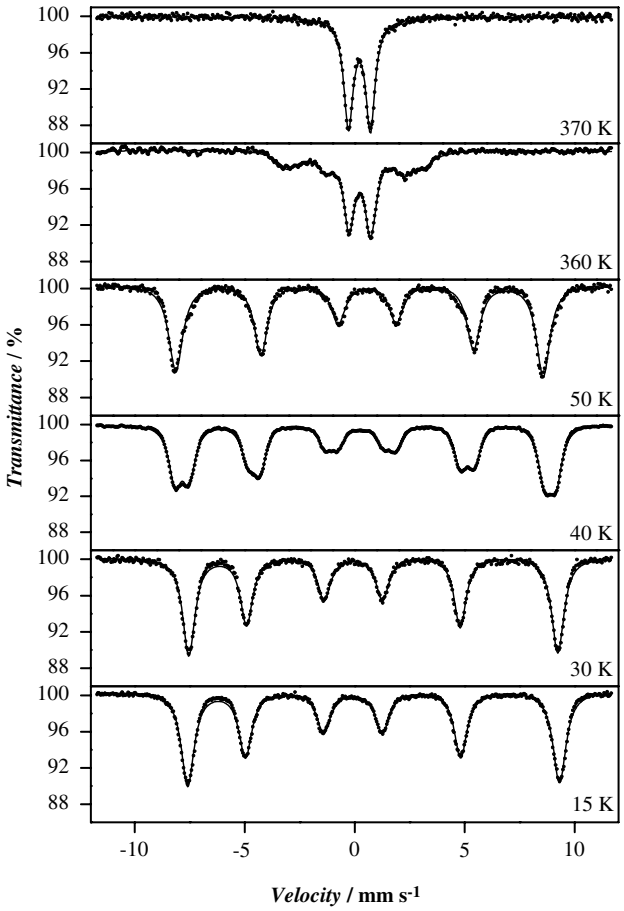

Figure 6. ^{57}Fe Mössbauer spectra of $CaNdFeO_4$ at 15, 30, 40, 50, 360 and 370 K.

the $3d^5$ electronic configuration are generally 0.15–0.5 mm s^{-1}. The isomer shift of the Fe^{3+} ion decreases with increasing temperature. This decrease should be attributable to a second-order Doppler (SOD) shift. According to the Debye model, the temperature dependence of the second-order Doppler shift $\Delta\delta_{SOD}$ can be expressed by the following equation [24]:

$$\Delta\delta_{SOD} = -\frac{9kT}{2Mc}\left\{\frac{1}{8}\frac{\Theta_D}{T} + \left(\frac{T}{\Theta_D}\right)^3 \int_0^{\Theta_D/T} \frac{x^3\,dx}{(e^x - 1)}\right\}, \tag{1}$$

where k is the Boltzmann's constant, Θ_D is the Debye temperature, and M and c are the mass of isotope and the speed of light, respectively. The theoretical curve with $\Theta_D = 470$ K obtained from equation (1) is in good agreement with the experimental data (see figure 7).

Figure 8 shows the temperature dependence of the magnetic hyperfine field determined for $CaNdFeO_4$ between 15 and 550 K. As seen in the figure, the H_{hf} versus T curve can be roughly reproduced by the molecular field approximation for $S = 5/2$. The magnetic ordering temperature of the Fe^{3+} sublattice in this compound is estimated to be around 370 K. The magnetic hyperfine field deduced was 0 K was 520 kOe, which was appropriate for the Fe^{3+} ion at the high-spin state. As shown in the inset of figure 8, an abnormal change in the H_{hf} versus T has been observed at 35 K, i.e., the magnetic hyperfine field shows a local dip

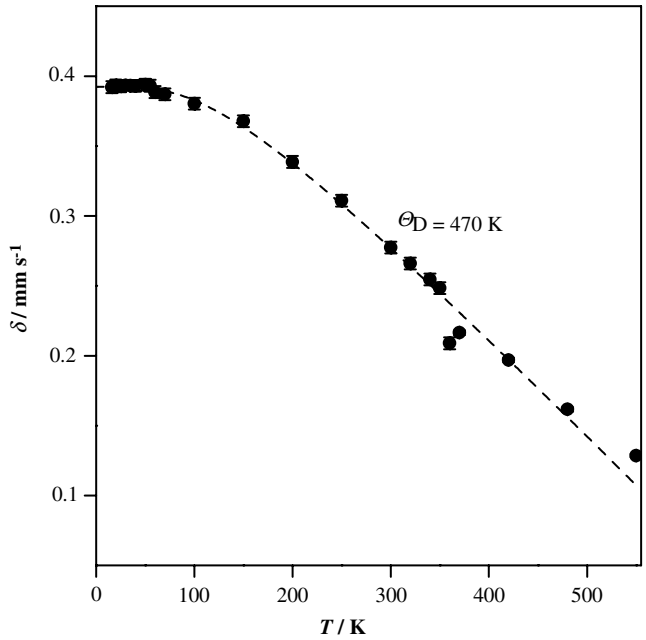

Figure 7. Temperature dependence of the isomer shifts of $CaNdFeO_4$.

at this temperature. This behaviour corresponds to the anomalies observed in the magnetic susceptibility and specific heat measurements. We consider that the above-mentioned abnormal variation of the magnetic hyperfine field with temperature is due to a spin-reorientation of the magnetic moments of the Fe^{3+} ions at 35 K.

Figure 9 shows the temperature dependence of the electric quadrupole splittings (ΔE_Q) in the temperature range between 15 and 550 K. The feature of the ΔE_Q–T curve is similar to that of $SrNdFeO_4$ [7]. The quadrupole splittings against temperature indicate that there exist three stages of spin states for the Fe^{3+} ions, depending on temperature:

Stage I:	$\Delta E_Q \sim 0.98\,\mathrm{mm\,s^{-1}},\ T > 370\,\mathrm{K}$	paramagnetic state,
Stage II:	$\Delta E_Q \sim -0.52\,\mathrm{mm\,s^{-1}}, 40\,\mathrm{K} < T < 370\,\mathrm{K}$	antiferromagnetic state,
Stage III:	$\Delta E_Q \sim 0.94\,\mathrm{mm\,s^{-1}}, T < 40\,\mathrm{K}$	antiferromagnetic state.

In the paramagnetic region (stage I), only the absolute value of ΔE_Q can be obtained from one doublet in the Mössbauer spectra, but the sign of ΔE_Q is confirmed to be positive from the magnetic structure of the Fe^{3+} moments, as will be shown later. This large positive quadrupole splitting is attributable to the strong axially distorted FeO_6 octahedron (see section 3.1). The quadrupole splitting for the paramagnetic state is given by [25]

$$\Delta E_Q = \frac{e^2qQ}{2}\left(1+\frac{1}{3}\eta^2\right)^{1/2}, \tag{2}$$

where eq is the value of the electric field gradient (EFG) along the maximum principal axis (the long axis of the FeO_6 octahedron) of EFG, Q is the nuclear quadrupole moment, and η is the asymmetry parameter of the EFG.

A magnetic ordering of the 3d electrons for the Fe^{3+} ion split the nuclear levels of ^{57}Fe through the contact and magnetic dipole interactions. If $e^2qQ \ll \mu H$, the quadrupole interaction can be treated as a first-order perturbation to the magnetic dipole interaction. As

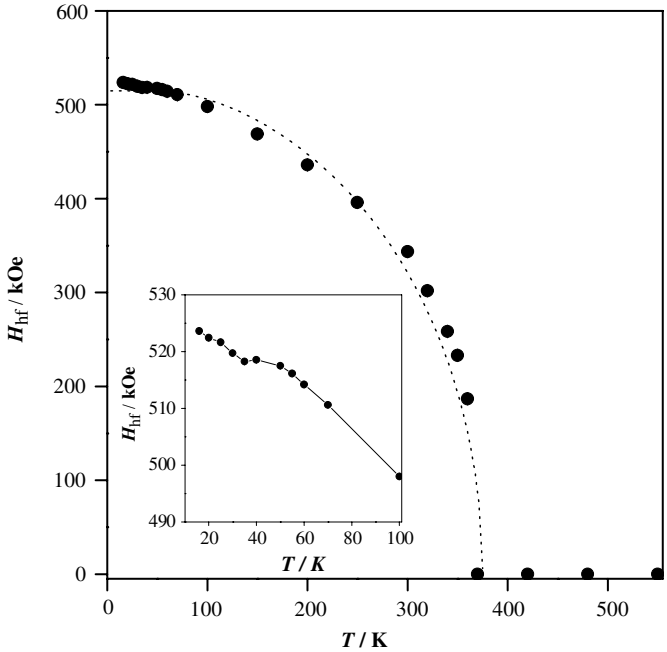

Figure 8. Temperature dependence of the magnetic hyperfine field of $CaNdFeO_4$. The inset shows the detailed temperature dependence at lower temperatures.

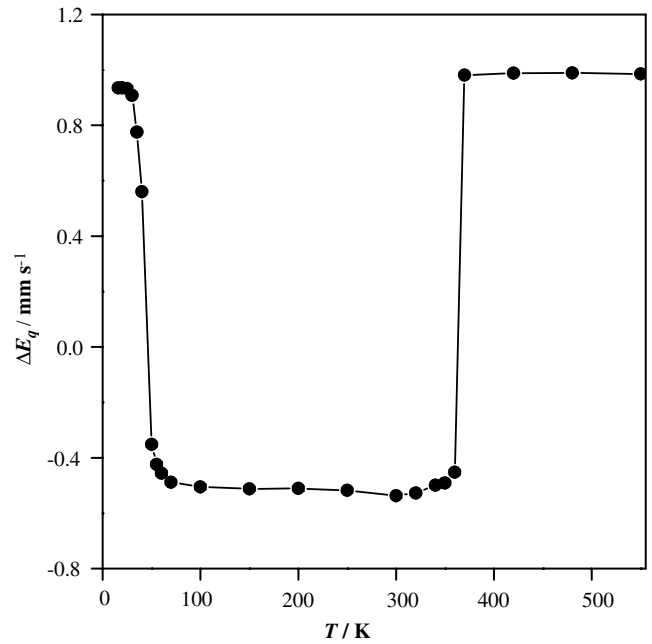

Figure 9. Temperature dependence of the electric quadrupole splitting (Δ) of $CaNdFeO_4$.

discussed in section 3.1, the symmetry of the crystal structure for $CaNdFeO_4$ is tetragonal at low temperatures. Therefore, the EFG tensor of the Fe^{3+} ion can be assumed to have approximate axial symmetry, and therefore the asymmetry parameter η can be approximated to zero. When the principal axis makes an angle θ with the magnetic axis, the energy eigenvalue ($E(m_I)$) of the nuclear sublevel with magnetic quantum number m_I is given by [26]

$$E(m_I) = -g_N \mu_N H m_I + (-1)^{|m_I|+(1/2)} \frac{e^2 qQ}{4} \left(\frac{3\cos^2\theta - 1}{2} \right), \tag{3}$$

where g_N and μ_N are the nuclear Landé g factor and nuclear magneton, respectively. Consequently, the effective quadrupole interaction (ΔE_{eff}) can be represented by the following relation:

$$\Delta E_{\text{eff}} = \frac{e^2 qQ}{2} \left(\frac{3\cos^2\theta - 1}{2} \right) = \Delta E_Q \left(\frac{3\cos^2\theta - 1}{2} \right). \tag{4}$$

From equation (4), $\Delta E_{\text{eff}} \sim -0.52\,\text{mm s}^{-1}$ in stage II and $\Delta E_{\text{eff}} \sim 0.94\,\text{mm s}^{-1}$ in stage III corresponds to the antiferromagnetic state with the spin direction of $\theta \sim 90^\circ$ and 10°, respectively. These results indicate that the magnetic moments of the Fe^{3+} ion lie on the *ab* plane in stage II and that they turn to the *c* direction in stage III.

The above-mentioned results were obtained by assuming the crystal structure of $CaNdFeO_4$ to have the tetragonal symmetry. In order to elucidate the accurate direction of magnetic moments for the Fe^{3+} ions, the magnetic structures of $CaNdFeO_4$ above and below the 'spin-reorientation temperature' were determined through the powder neutron diffraction measurements.

3.4. Magnetic structures

Powder neutron diffraction data were collected in the temperature range between 2.5 K and room temperature. The diffraction profiles at 2.5 and 60 K are shown in figure 10. In all the profiles below room temperature, the magnetic Bragg reflections appear and have been indexed on the basis of a propagation vector $\boldsymbol{k} = [0\,0\,0]$. This result indicates that the magnetic moments of the Fe^{3+} ion in $CaNdFeO_4$ have a long-range ordering and that the magnetic unit cell is equal to the nuclear unit cell. Figure 11 shows the temperature dependence of the integrated intensity of some magnetic Bragg reflections. Below 50 K, abrupt changes in the intensities are observed with decrease in temperature. These changes correspond to the anomalies observed in the magnetic susceptibility, specific heat, and ^{57}Fe Mössbauer spectrum measurements, and they are ascribed to the spin-reorientation of the Fe^{3+} magnetic moments.

We have considered the magnetic structure of the Fe^{3+} ions by using the representation analysis [27]. The Fe^{3+} ions occupy the following Wyckoff 4*a* sites of the space group Bmab.

Position	x	y	z
Fe1	0	0	0
Fe2	1/2	0	1/2
Fe3	0	1/2	1/2
Fe4	1/2	1/2	0

with respective spin vectors $\boldsymbol{S}_1$, $\boldsymbol{S}_2$, $\boldsymbol{S}_3$, and $\boldsymbol{S}_4$. In the case of the propagation vector $\boldsymbol{k} = [0\,0\,0]$, we can find one ferromagnetic and three antiferromagnetic arrangements as listed in table 3. The rules for the allowed magnetic reflections are also listed in table 3. When we take as independent symmetry elements the B centring translation $t = (\frac{1}{2}\,0\,\frac{1}{2})$, the 2-fold screw axis

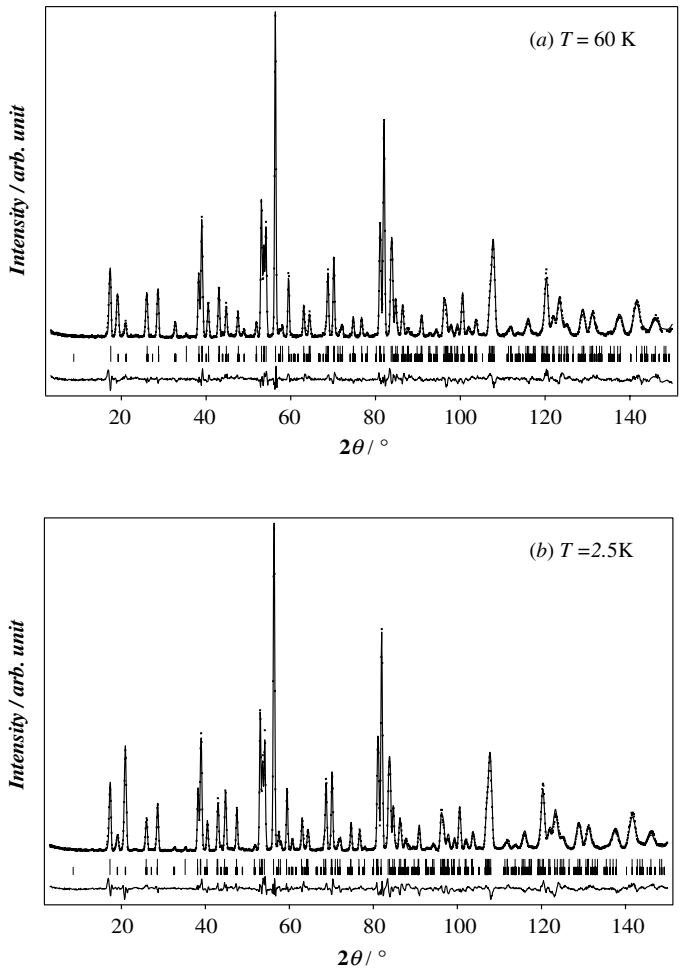

Figure 10. Powder neutron diffraction profiles for $CaNdFeO_4$ at 60 K (a) and 2.5 K (b). The calculated and observed diffraction profiles are shown by the top solid line and the cross markers, respectively. The nuclear reflection positions are shown by upper vertical markers and magnetic positions are shown by lower ones. The lower trace is a plot of the difference between calculated and observed intensities.

2_{1y}, and the 2-fold rotation axis 2_z, the basis vectors for the irreducible representations of the space group Bmab are given by the linear combinations of the spin components as shown in table 4.

If the crystal structure has a pseudo-tetragonal symmetry, it is often difficult to distinguish between the *G*- and *F*-type magnetic structure because of the overlap between the *hkl* and *khl* reflections [13, 28]. In the case of $CaNdFeO_4$, due to the large orthorhombic distortion from the tetragonal symmetry above 100 K, we can determine that the magnetic structure is of the *G*-type from the selection rules for the magnetic reflections. For the profiles above 50 K, the model for the $\Gamma_4(-++)$ representation with $A_z = 0$ gives the best fit of the Rietveld refinement as shown in figure 10(a). Table 5 lists the refined crystallographic and magnetic parameters at 60 K. The collinear magnetic structure of the G_y mode is illustrated in figure 12(a). The Fe^{3+} magnetic moments orient along the *b*-axis.

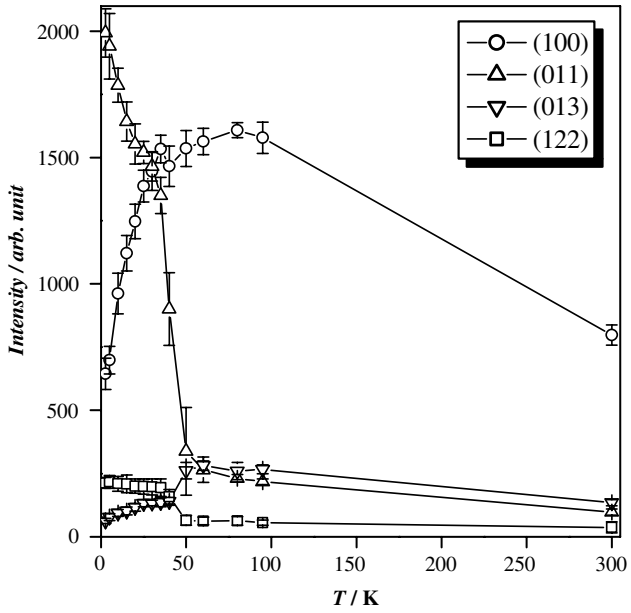

Figure 11. Temperature dependence of the integrated intensities of some magnetic Bragg reflections for $CaNdFeO_4$.

Table 3. Rules for allowed magnetic reflections.

	Rules for allowed magnetic reflections		
Magnetic structure	$h+l$	$k+l$	$h+k$
$F = S_1 + S_2 + S_3 + S_4$	Even	Even	Even
$G = S_1 - S_2 + S_3 - S_4$	Odd	Even	Odd
$C = S_1 + S_2 - S_3 - S_4$	Even	Odd	Odd
$A = S_1 - S_2 - S_3 + S_4$	Odd	Odd	Even

Table 4. Representations of the base vectors.

Representation				Magnetic group
$\Gamma_1(+++)$	C_x	–	–	Bmab
$\Gamma_2(++-)$	–	F_y	C_z	Bm′ab
$\Gamma_3(+-+)$	–	C_y	F_z	Bm′a′b
$\Gamma_4(-++)$	–	G_y	A_z	B_pm′a′b′
$\Gamma_5(+--)$	F_x	–	–	Bma′b′
$\Gamma_6(-+-)$	A_x	–	–	$B_p$ma′b
$\Gamma_7(--+)$	G_x	–	–	$B_p$mab′
$\Gamma_8(---)$	–	A_y	G_z	B_pm′ab

The reflection conditions for the profiles below 35 K also fulfil those for the G-type magnetic structure. However, the direction of the magnetic moments changes from the G_y mode above 50 K to the G_z mode for the $\Gamma_8(---)$ representation with $A_y = 0$. This 'spin reorientation' from the G_y mode to the G_z mode is consistent with the variation of

Table 5. Crystal and magnetic data determined by neutron diffraction measurements at 60 and 2.5 K for CaNdFeO4.

	Site	x	y	z	B (Å^2)
60 K					
Ca,Nd	8f	0	−0.0141(3)	0.3576(2)	0.42(5)
Fe	4a	0	0	0	0.56(5)
O(1)	8e	0.25	0.25	−0.0151(3)	0.66(5)
O(2)	8f	0	0.0548(5)	0.1732(3)	0.66
2.5 K					
Ca,Nd	8f	0	−0.0131(2)	0.3578(5)	0.21(5)
Fe	4a	0	0	0	0.83(5)
O(1)	8e	0.25	0.25	−0.0175(2)	0.99(7)
O(2)	8f	0	0.0549(3)	0.1726(2)	0.99

Space group: Bmab (No. 64)
60 K: $R_{wp} = 12.6\%$, $R_{Bragg} = 6.17\%$, $R_{mag} = 12.6\%$
$a = 5.4468(1)$ Å, $b = 5.4617(2)$ Å, $c = 12.0037(5)$ Å
$m(Fe^{3+}) = 3.84(7)\mu_B$
2.5 K: $R_{wp} = 13.6\%$, $R_{Bragg} = 6.38\%$, $R_{mag} = 10.4\%$
$a = 5.4422(9)$ Å, $b = 5.4599(2)$ Å, $c = 11.9939(2)$ Å
$m(Fe^{3+}) = 4.19(4)\mu_B$, $m(Nd^{3+}) = 1.85(7)\mu_B$

Note: $R_{wp} = \left[\sum w(|F(\text{obs})| - |F(\text{cal})|)^2 / \sum w|F(\text{obs})|^2\right]^{1/2}$.
$R_{Bragg} = \sum |I(\text{obs}) - I(\text{cal})| / \sum I(\text{obs})$.
$R_{mag} = \sum |I_{mag}(\text{obs}) - I_{mag}(\text{cal})| / \sum I_{mag}(\text{obs})$.

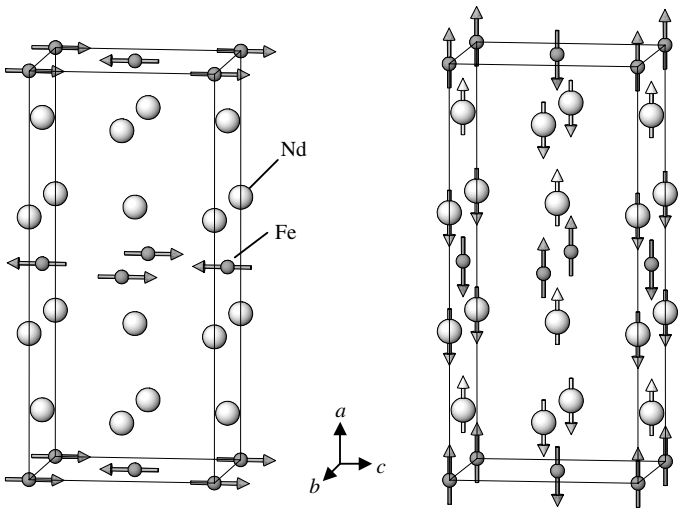

Figure 12. Magnetic structure models of $CaNdFeO_4$ above 50 K (a) and below 35 K (b). Oxide ions are omitted. Nd^{3+} and Ca^{2+} ions are randomly distributed in the same site. The directions of the magnetic moments are shown.

the quadrupole splittings for the ^{57}Fe Mössbauer spectra as described in section 3.3. For the profiles below 40 K, the changes in the integrated intensities of the magnetic Bragg reflections can be explained by assuming magnetic ordering of the Nd^{3+} sublattice in addition to the

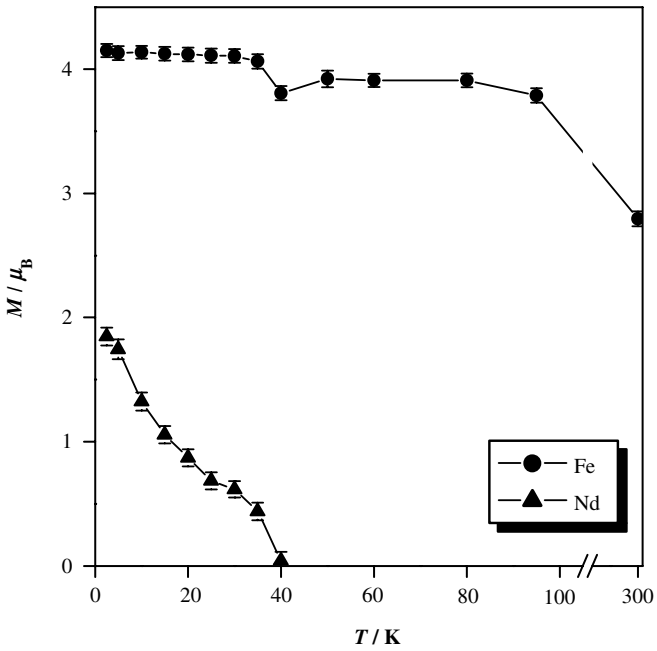

Figure 13. Temperature dependence of the ordered magnetic moments of Fe^{3+} and Nd^{3+} ions.

contribution of the spin-reorientation for the Fe^{3+} moment. The Nd^{3+} moments have been found to orient also along the c-axis. The calculated and observed diffraction profiles at 2.5 K are shown in figure 10(b) and the refined crystallographic and magnetic parameters at 2.5 K are listed in table 5. The presence of weak ferromagnetic components observed in the magnetic susceptibilities below 35 K is suggestive of a noncollinear magnetic structure. However, no magnetic reflection due to the F mode of the Fe^{3+} and Nd^{3+} moments has been detected in the obtained profiles because the ferromagnetic components are very small. Figure 12(b) illustrates the collinear magnetic structure of the predominant G_z mode below 35 K.

Figure 13 shows the ordered magnetic moments of the Fe^{3+} and Nd^{3+} ions as a function of temperature. The Fe^{3+} ordered moment decreases gradually with increase in temperature and the thermal fluctuation reduces the ordered moment to ∼67% when the temperature is at 300 K. This reduction of ∼33% in the Fe^{3+} ordered moment is in good agreement with the ∼34% reduction at room temperature in the internal magnetic field H_{hf} of the Fe^{3+} ions observed by the ^{57}Fe Mössbauer spectrum measurements. Below 35 K, a slight enhancement of the Fe^{3+} ordered moment has been observed. We consider that this enhancement results from the magnetic ordering of the Nd^{3+} ions when the temperature is decreased below 35 K. However, the ordered moment ($4.15\mu_B$) at 2.5 K is smaller than the observed Fe^{3+} moments ($4.5–4.6\mu_B$) in the orthoferrites $LnFeO_3$ (Ln = rare-earths) which form into a three-dimensional corner-sharing network of the FeO_6 octahedra [29]. It has been discussed that the difference between the expected moment $gS = 5\mu_B$ and the moments of $4.5–4.6\mu_B$ in $LnFeO_3$ could be attributable to the covalency effect. The larger difference in the ordered moments between the expected moment and the experimental moment for the $CaNdFeO_4$ indicates that in addition to the covalency effect, there exists a large zero-point spin deviation for a two-dimensional lattice. The ordered moment of Fe^{3+} at 2.5 K in the $CaNdFeO_4$ ($4.15\mu_B$) is comparable to

those for other Fe^{3+} oxides with K_2NiF_4-type structure ($4.23\mu_B$ at 4.2 K for $SrLaFeO_4$ [30], $4.24\mu_B$ at 2.3 K for $SrNdFeO_4$ [7], and $3.74\mu_B$ at 4.2 K for $CaLaFeO_4$ [15]).

The ordering of the Nd^{3+} moment occurs when the temperature is decreased below 40 K and the ordered moment increases with decrease in temperature. However, the value of the Nd^{3+} ordered moment ($1.85\mu_B$) at 2.5 K is pronouncedly smaller than the theoretical moment $g_J J = 3.27\mu_B$ for the $^4I_{9/2}$ ground state of a Nd^{3+} free ion, and is slightly smaller than that ($2.45\mu_B$) for $SrNdFeO_4$ [7]. This large reduction of the ordered Nd^{3+} moment should be mainly attributable to the crystal field effect and it is supposed that the low-lying doublet of the Nd^{3+} ion forms predominantly the antiferromagnetic state of the Nd^{3+} moments.

It is worth noting that the temperature at which the Nd^{3+} moments magnetically order coincides with the spin-reorientation transition temperature of Fe^{3+} moments. This fact indicates that the spin-reorientation of the Fe^{3+} sublattices could be induced by the onset of local magnetic interactions between Nd^{3+} and Fe^{3+} ions.

Acknowledgment

The authors are indebted to the Japan Securities Scholarship Foundation for financial support.

References

[1] Balz D and Pleith K 1955 *Z. Elektrochem.* **59** 545
[2] Birgeneau R J, Guggenheim H J and Shirane G 1969 *Phys. Rev. Lett.* **22** 720
[3] Birgeneau R J, DeRosa F and Guggenheim H J 1970 *Solid State Commun.* **8** 13
[4] Suzuki T and Fujita T 1989 *Physica* C **159** 111
[5] Lander G H, Brown P J, Spalek J and Honig J H 1989 *Phys. Rev.* B **40** 4463
[6] Aleksandrov K 1987 *Sov. Phys. Crystallogr.* **32** 551
[7] Oyama S, Wakeshima M, Hinatsu Y and Ohoyama K 2004 *J. Phys.: Condens. Matter* **16** 1823–36
[8] Jantzen C M and Glasser F P 1979 *Mater. Res. Bull.* **14** 1601
[9] Fava J, Danot M, trut Dinh N, Daoudi A, Le Flem G and Fabritchnyi P B 1977 *Solid State Commun.* **22** 733
[10] Izumi F and Ikeda T 2000 *Mater. Sci. Forum* **198** 321
[11] Ohoyama K, Kanouchi T, Nemoto K, Ohashi M, Kajitani T and Yamaguchi Y 1998 *Japan J. Appl. Phys.* **37** 3319
[12] Rodriguez-Carvajal J 1993 *Physica* B **192** 55
[13] Romero de Paz J, Hernández Velacco J, Fernández-Díaz M T, Porcher P, Martínez J L and Sáez Puche R 1999 *J. Solid State Chem.* **148** 361
[14] Rodríguez-Carvajal J, Martínez J L, Pannetier J and Saez-Puche R 1988 *Phys. Rev.* B **38** 7148
[15] Nguyen-Trut-Dinh M M, Vlasse M, Perrin M and Le Flem G 1980 *J. Solid State Chem.* **32** 1
[16] Sun K, Cho J H, Chou F C, Lee W C, Miller L L, Jhonston D C, Hidaka Y and Murakami T 1991 *Phys. Rev.* B **43** 239
[17] Sengupta P, Sandvik A W and Singh R 2003 *Phys. Rev.* B **68** 094423
[18] Van Vleck J H 1932 *Theory of Electric and Magnetic Susceptibilities* (Oxford: Clarendon)
[19] Oyama S, Wakeshima M and Hinatsu Y, unpublished data
[20] Levinson J M and Shtrikman S 1970 *Solid State Commun.* **8** 209
[21] Bartolomé J, Palacios E, Kuz'min M D, Bartolomé F, Sosnowska I, Przenios ło R, Sonntag R and Lukina M M 1997 *Phys. Rev.* B **55** 11432
[22] Bartolomé F, Bartolomé J, Castro M and Melero J J 2000 *Phys. Rev.* B **62** 1058
[23] Tezuka K and Hinatsu Y 2001 *J. Solid State Chem.* **160** 362
[24] McCammon C 1996 *Phase Transitions* **58** 1
[25] Uhm Y R and Kim C S 2001 *J. Appl. Phys.* **89** 7344
[26] Hector A L, Hutchings J A, Needs R L, Thomas M F and Weller M T 2001 *J. Mater. Chem.* **11** 527
[27] Bertaut E F 1963 *Magnetism* vol III, ed G T Rado and Suhl H (New York: Academic) ch 4
[28] Romero de Paz J, Fernández-Díaz M T, Hernández Velacco J, Sáez Puche R and Martínez J L 1999 *J. Solid State Chem.* **142** 29
[29] Koehler W C, Wollan E O and Wilkinson M K 1960 *Phys. Rev.* **118** 58
[30] Soubeyroux J L, Courbin P, Fournes L, Fruchart D and Le Flem G 1980 *J. Solid State Chem.* **31** 313